

Joint Polarization/Waveform Design and Adaptive Receive Processing

Patrick McCormick¹, John Jakabosky¹, Shannon D. Blunt¹, Chris Allen¹, and Braham Himed²

¹Radar Systems Lab, University of Kansas, Lawrence, KS

²Sensors Directorate, Air Force Research Laboratory, Dayton, OH

Abstract—Leveraging the design freedom provided by the recently developed polyphase-coded FM (PCFM) waveform structure and the enhanced sensitivity on receive through sidelobe suppression provided by adaptive pulse compression (APC) and its variants, the impact on full polarimetric scattering estimation is examined. By incorporating a Σ - Δ hybrid combiner different polarization modulation schemes are considered. To address the limitation on achievable cross-correlation between the waveforms associated with orthogonal polarization channels, a polarimetric adaptive pulse compression (PAPC) method is derived that is used to isolate adaptively the different polarization components. Results from an open-air experiment are provided to demonstrate the efficacy of PAPC with this new emission structure. A decoupled emission structure is also tested to use as a benchmark for comparison.

I. INTRODUCTION

In [1] it was shown that arbitrary polyphase codes could be implemented as physical waveforms using a modified version of Continuous Phase Modulation (CPM) [2] thereby allowing for transmission using a saturated high-power amplifier with minimal distortion. These polyphase-coded FM (PCFM) waveforms can likewise be optimized specific to the hardware distortion [3]. Here this framework is examined as a means to modulate polarization in fast-time as well.

The notion of using polarization to improve radar performance is not new (see [4] and references therein) and is implemented regularly in weather radar [5] and polarimetric SAR systems [6]. Polarization diversity, in its simplest form, uses two orthogonally polarized antennas to achieve a fully polarimetric system for transmission and/or reception. The amplitude and/or phase difference between the orthogonal emissions controls the state of polarization. The state of polarization can be described as, but is not limited to, either a spherical mapping onto the Poincaré sphere or the two-dimensional polarization ellipse.

The change in polarization that occurs when an incident plane wave is reflected can be characterized using the complex 2×2 scattering matrix. The determination of the scattering parameters can be found through the use of adequately separable emissions transmitted from the orthogonally polarized antennas. These emissions can be separated in time, frequency, or by using distinct waveform modulations, where the appeal of the latter is the efficient use of time and frequency. However, the efficacy of using separable waveform modulations for determining scattering parameters is limited by the cross-correlation between the waveforms transmitted from the orthogonally polarized

antennas. Further, since the environment tends to be comprised of a collection of scatterers with various polarization attributes, these waveforms must generally possess low cross-correlation over all possible delay shifts (hence truly orthogonal waveforms are not possible).

The continuous nature of a PCFM waveform provides the ability to control the instantaneous polarization of the emission and through the use of a Σ - Δ hybrid combiner different polarization states can be achieved. The emission schemes investigated here include the examination of fast-time polarization control and the implementation of low cross-correlation waveforms (similar to [7,8]).

The received processing is examined using matched filtering, which is limited by the cross-correlation of the waveforms, and with a variant of Multistatic Adaptive Pulse Compression (MAPC) [9] developed specifically for dual-polarized radar that is denoted as polarimetric adaptive pulse compression (PAPC). On receive, the PAPC algorithm adaptively enhances the separability of the waveforms by suppressing both co-polar and cross-polar sidelobes. This sidelobe suppression opens the door for a variety of different emission structures that are possible through polarization modulation and increases the effective dynamic range relative to traditional matched filtering.

To demonstrate the efficacy of the receive processing for real sensing applications open-air experiments were performed using co-located, dual-polarized Vivaldi antennas for simultaneous transmit and receive using a corner reflector as the scatterer. The corner reflector assumed the shape of a trihedral and dihedral at different tilt angles. The matched filter and PAPC estimates are compared against a time-separated transmission with very low range sidelobes [10] which provides decoupled estimates of the scattering parameters with high sensitivity. Each estimated scattering matrix is compared to the ideal normalized scattering matrices of the two reflector arrangements.

II. POLARIZATION MODULATION

A dual-polarized emission requires two waveforms, here denoted as $s_1(t)$ and $s_2(t)$ having time support on $[0, T]$ with T the pulsewidth. The cross-polarized antenna elements may, for example, be a pair of crossed dipoles co-aligned with the vertical and horizontal axes having the respective emissions $s_v(t)$ and $s_h(t)$. It is generally desirable that these waveforms have a low cross-correlation to allow for separation of co-pole and cross-pole scattering on receive [7,8].

Leveraging recent work to control the rise/fall-times of waveforms for spectral containment at high power [11], consider fast-time polarization modulation through the use of

This work was supported in part by a subcontract with Booz, Allen and Hamilton for research sponsored by the Air Force Research Laboratory under Contract FA8650-11-D-1011 and by the Air Force Office of Scientific Research.

a Σ - Δ hybrid where the two input waveforms $s_1(t)$ and $s_2(t)$ are combined as

$$s_H(t) = \frac{1}{\sqrt{2}}(s_1(t) + s_2(t)) \quad (1)$$

$$s_V(t) = \frac{1}{\sqrt{2}}(s_2(t) - s_1(t))\exp(j\kappa) \quad (2)$$

to generate the horizontally and vertically polarized emissions (Fig. 1). For the case in which the waveforms are constant modulus the sum and difference of the two waveforms controls the tilt angle χ and/or ellipticity angle ε of the polarization ellipse (Fig. 2) and the ability to modulate on the Poincaré sphere. The variable κ is an additional phase term used to set the region of feasible modulation corresponding to a particular great circle on the Poincaré sphere. For example, if $\kappa = 0$ then $\chi = 0, \pm\pi/2$ with ε variable (Fig. 3a) or if $\kappa = -\pi/2$ then $\varepsilon = 0$ with χ variable (Fig. 3b). Since the amplitudes of $s_H(t)$ and $s_V(t)$ vary during the pulse due to the sum/difference combining, power amplification must be performed prior to the Σ - Δ hybrid in order to use high-efficiency power amplifiers (operated in saturation).

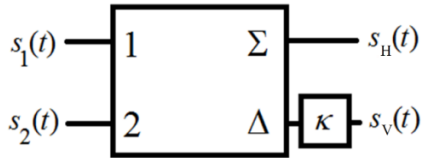


Figure 1. Σ - Δ hybrid for polarization control

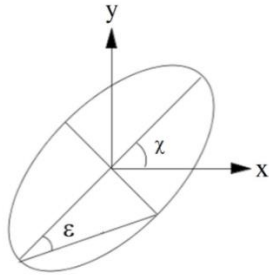


Figure 2. Polarization ellipse

An additional emission is considered for the case in which the hybrid is removed and the waveforms $s_1(t)$ and $s_2(t)$ are directly connected to $s_H(t)$ and $s_V(t)$, respectively. This structure is the traditional means of transmitting low cross-correlated waveforms [7,8]. Similar to Figs. 3a and 3b, the emission is constrained to the great circle that corresponds to the resulting horizontal and vertical emissions being constant modulus (Fig. 3c).

These polarization constraints occur due to the lack of degrees of freedom when operating with constant modulus waveforms, where the phase between the waveforms is the only degree of control. Any polarization may be realized with a variable phase shift κ , though here κ is assumed to be fixed.

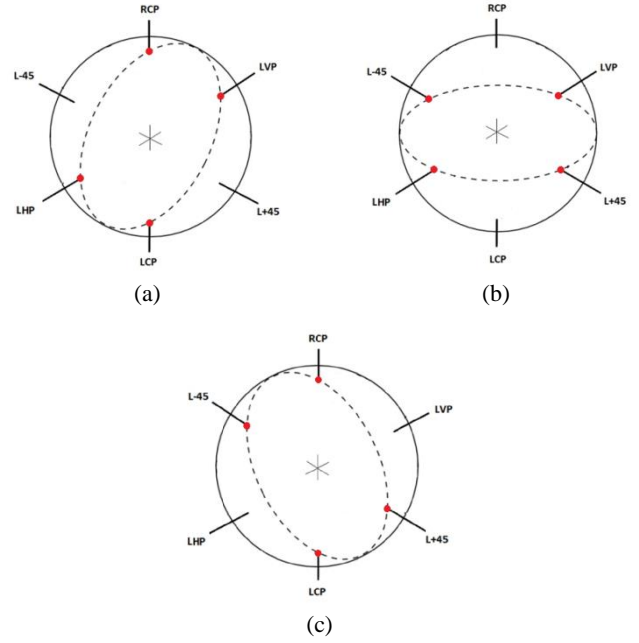


Figure 3. Feasible polarization modulations on the Poincaré sphere for a) $\kappa = 0$; b) $\kappa = -\pi/2$ and c) no hybrid. RCP: right-hand circular, LCP: left-hand circular, LHP: linear horizontal, LVP: linear vertical, L-45: linear with -45° tilt, L+45: linear with $+45^\circ$ tilt

A PCFM waveform is implemented from a length $N + 1$ arbitrary polyphase code via [1]. To perform polarization modulation using this structure, two length $N + 1$ polyphase codes are needed. Define these phase codes as $\phi_0, \phi_1, \dots, \phi_N$ and $\psi_0, \psi_1, \dots, \psi_N$. Using the PCFM implementation of [1], a train of N impulses with time separation T_p are formed so that the total pulsewidth is $T = NT_p$. Here the phase variable ϕ (for $-\pi \leq \phi \leq \pi$) controls the waveform phase and ψ (for $-\pi/2 \leq \psi \leq \pi/2$) controls the polarization state of the emission. The n^{th} impulse is weighted by α_n and β_n , which are defined as

$$\alpha_n = \begin{cases} \tilde{\alpha}_n & \text{if } |\tilde{\alpha}_n| \leq \pi \\ \tilde{\alpha}_n - 2\pi \operatorname{sgn}(\tilde{\alpha}_n) & \text{if } |\tilde{\alpha}_n| > \pi \end{cases} \quad (3)$$

$$\beta_n = \begin{cases} \tilde{\beta}_n & \text{if } |\tilde{\beta}_n| \leq \pi/2 \\ \tilde{\beta}_n - \pi \operatorname{sgn}(\tilde{\beta}_n) & \text{if } |\tilde{\beta}_n| > \pi/2 \end{cases}, \quad (4)$$

where

$$\tilde{\alpha}_n = \phi_n - \phi_{n-1} \quad \text{for } n = 1, \dots, N \quad (5)$$

$$\tilde{\beta}_n = \psi_n - \psi_{n-1} \quad \text{for } n = 1, \dots, N, \quad (6)$$

and $\operatorname{sgn}(\bullet)$ is the sign operation.

The resulting PCFM waveforms that enable polarization modulation using (1) and (2) via the Σ - Δ hybrid are thus

$$s_1(t) = \exp \left\{ j \left[\int_0^t g(\tau) * \left[\sum_{n=1}^N (\alpha_n + \beta_n) \delta(\tau - (n-1)T_p) \right] d\tau + \phi_0 + \psi_0 \right] \right\} \quad (7)$$

$$s_2(t) = \exp \left\{ j \left(\int_0^t g(\tau) * \left[\sum_{n=1}^N (\alpha_n - \beta_n) \delta(\tau - (n-1)T_p) \right] d\tau + \phi_0 - \psi_0 \right) \right\} \quad (8)$$

where * denotes convolution, $(\phi_0 + \psi_0)$ and $(\phi_0 - \psi_0)$ comprise the initial phase values of the codes, and $\delta(t)$ is an impulse function. The shaping filter $g(t)$ has the requirements 1) that it integrates to unity over the real line; and 2) that it has time support on $[0, T_p]$.

III. RECEIVE PROCESSING

Define the dual-polarized scattering matrix as a function of time (delay) as

$$X(t) = \begin{bmatrix} x_{\text{HH}}(t) & x_{\text{HV}}(t) \\ x_{\text{VH}}(t) & x_{\text{VV}}(t) \end{bmatrix}. \quad (9)$$

The discretized dual-polarized received signal can therefore be expressed as

$$y_{\text{H}}(\ell) = \mathbf{x}_{\text{HH}}^T(\ell) \mathbf{s}_{\text{H}} + \mathbf{x}_{\text{HV}}^T(\ell) \mathbf{s}_{\text{V}} + u_{\text{H}}(\ell) \quad (10)$$

$$y_{\text{V}}(\ell) = \mathbf{x}_{\text{VH}}^T(\ell) \mathbf{s}_{\text{H}} + \mathbf{x}_{\text{VV}}^T(\ell) \mathbf{s}_{\text{V}} + u_{\text{V}}(\ell), \quad (11)$$

where the length M vectors \mathbf{s}_{H} and \mathbf{s}_{V} are discretized versions of the emissions $s_{\text{H}}(t)$ and $s_{\text{V}}(t)$ for some degree of “over-sampling” relative to 3 dB bandwidth and $(\bullet)^T$ is the transpose operation. The terms $u_{\text{H}}(t)$ and $u_{\text{V}}(t)$ represent zero-mean, white Gaussian noise that is present at discrete delay ℓ on the horizontal and vertical receive channels, respectively. It is the four scattering responses in (9) that we wish to estimate based on the observed signals (10) and (11).

The degree of “over-sampling” with respect to the 3-dB bandwidth is denoted by the integer K . Therefore, the time-bandwidth product is approximately $BT = M/K$. Further details on this “over-sampling” can be found in [1, 12].

Collecting M contiguous samples of (10) and (11) into the vectors $\mathbf{y}_{\text{H}}(\ell)$ and $\mathbf{y}_{\text{V}}(\ell)$ respectively, the matched filter estimates of the four scattering responses can be written as

$$\hat{x}_{\text{HH}}(\ell) = \mathbf{s}_{\text{H}}^H \mathbf{y}_{\text{H}}(\ell) \quad (12)$$

$$\hat{x}_{\text{HV}}(\ell) = \mathbf{s}_{\text{V}}^H \mathbf{y}_{\text{H}}(\ell) \quad (13)$$

$$\hat{x}_{\text{VH}}(\ell) = \mathbf{s}_{\text{H}}^H \mathbf{y}_{\text{V}}(\ell) \quad (14)$$

$$\hat{x}_{\text{VV}}(\ell) = \mathbf{s}_{\text{V}}^H \mathbf{y}_{\text{V}}(\ell) \quad (15)$$

where $(\bullet)^H$ is the complex-conjugate transpose. Clearly these estimates will be contaminated by the non-zero cross-correlations between the horizontal and vertical emissions.

Polarimetric adaptive pulse compression (PAPC) is devised to separate the aggregation of received signals occupying the same spectrum. A unique filter is generated for each range delay of each transmit/receive polarization pair that has the ability to suppress co-pole/cross-pole range sidelobe interference thus enhancing sensitivity over traditional matched filtering.

It has been found that for FM waveforms, APC and its variants are more robust to straddling effects [12] when implemented using the decimated version of fast adaptive pulse compression (FAPC) [13], with the decimation equal to the over-sampling factor K . This structure is adopted here as well. The PAPC receive filter for range index ℓ for each scattering response is found by minimizing a gain-constrained minimum mean-square error (MMSE) cost function for each of the four polarized scattering responses:

$$\tilde{J}_{\text{HH}}(\ell) = \sum_{k=0}^{K-1} E \left[\left| \frac{1}{K} x_{\text{HH}}(\ell) - \tilde{\mathbf{w}}_{k,\text{HH}}^H(\ell) \tilde{\mathbf{y}}_{k,\text{H}}(\ell) \right|^2 \right] + \text{Re} \left\{ \lambda \left(\sum_{k=0}^{K-1} (\tilde{\mathbf{w}}_{k,\text{HH}}^H(\ell) \tilde{\mathbf{s}}_{k,\text{H}}) - 1 \right) \right\} \quad (16)$$

$$\tilde{J}_{\text{HV}}(\ell) = \sum_{k=0}^{K-1} E \left[\left| \frac{1}{K} x_{\text{HV}}(\ell) - \tilde{\mathbf{w}}_{k,\text{HV}}^H(\ell) \tilde{\mathbf{y}}_{k,\text{H}}(\ell) \right|^2 \right] + \text{Re} \left\{ \lambda \left(\sum_{k=0}^{K-1} (\tilde{\mathbf{w}}_{k,\text{HV}}^H(\ell) \tilde{\mathbf{s}}_{k,\text{V}}) - 1 \right) \right\} \quad (17)$$

$$\tilde{J}_{\text{VH}}(\ell) = \sum_{k=0}^{K-1} E \left[\left| \frac{1}{K} x_{\text{VH}}(\ell) - \tilde{\mathbf{w}}_{k,\text{VH}}^H(\ell) \tilde{\mathbf{y}}_{k,\text{V}}(\ell) \right|^2 \right] + \text{Re} \left\{ \lambda \left(\sum_{k=0}^{K-1} (\tilde{\mathbf{w}}_{k,\text{VH}}^H(\ell) \tilde{\mathbf{s}}_{k,\text{H}}) - 1 \right) \right\} \quad (18)$$

$$\tilde{J}_{\text{VV}}(\ell) = \sum_{k=0}^{K-1} E \left[\left| \frac{1}{K} x_{\text{VV}}(\ell) - \tilde{\mathbf{w}}_{k,\text{VV}}^H(\ell) \tilde{\mathbf{y}}_{k,\text{V}}(\ell) \right|^2 \right] + \text{Re} \left\{ \lambda \left(\sum_{k=0}^{K-1} (\tilde{\mathbf{w}}_{k,\text{VV}}^H(\ell) \tilde{\mathbf{s}}_{k,\text{V}}) - 1 \right) \right\} \quad (19)$$

where the $\text{Re}\{\bullet\}$ term constrains the gain of each filter to unity per [14]. The k th filter for each co-pole and cross-pole term, for $k = 1, 2, \dots, K$, yields

$$\tilde{\mathbf{w}}_{k,\text{HH}}(\ell) = \frac{(\tilde{\mathbf{C}}_{k,\text{HH}}^z(\ell) + \tilde{\mathbf{C}}_{k,\text{HV}}(\ell) + \tilde{\mathbf{R}}_{k,\text{H}})^{-1} \tilde{\mathbf{s}}_{k,\text{H}}}{\sum_{i=0}^{K-1} \tilde{\mathbf{s}}_{i,\text{H}}^H (\tilde{\mathbf{C}}_{i,\text{HH}}^z(\ell) + \tilde{\mathbf{C}}_{i,\text{HV}}(\ell) + \tilde{\mathbf{R}}_{i,\text{H}})^{-1} \tilde{\mathbf{s}}_{i,\text{H}}} \quad (20)$$

$$\tilde{\mathbf{w}}_{k,\text{HV}}(\ell) = \frac{(\tilde{\mathbf{C}}_{k,\text{HH}}(\ell) + \tilde{\mathbf{C}}_{k,\text{HV}}^z(\ell) + \tilde{\mathbf{R}}_{k,\text{H}})^{-1} \tilde{\mathbf{s}}_{k,\text{V}}}{\sum_{i=0}^{K-1} \tilde{\mathbf{s}}_{i,\text{V}}^H (\tilde{\mathbf{C}}_{i,\text{HH}}(\ell) + \tilde{\mathbf{C}}_{i,\text{HV}}^z(\ell) + \tilde{\mathbf{R}}_{i,\text{H}})^{-1} \tilde{\mathbf{s}}_{i,\text{V}}} \quad (21)$$

$$\tilde{\mathbf{w}}_{k,\text{VH}}(\ell) = \frac{(\tilde{\mathbf{C}}_{k,\text{VH}}^z(\ell) + \tilde{\mathbf{C}}_{k,\text{VV}}(\ell) + \tilde{\mathbf{R}}_{k,\text{V}})^{-1} \tilde{\mathbf{s}}_{k,\text{H}}}{\sum_{i=0}^{K-1} \tilde{\mathbf{s}}_{i,\text{H}}^H (\tilde{\mathbf{C}}_{i,\text{VH}}^z(\ell) + \tilde{\mathbf{C}}_{i,\text{VV}}(\ell) + \tilde{\mathbf{R}}_{i,\text{V}})^{-1} \tilde{\mathbf{s}}_{i,\text{H}}} \quad (22)$$

$$\tilde{\mathbf{w}}_{k,\text{VV}}(\ell) = \frac{(\tilde{\mathbf{C}}_{k,\text{VH}}(\ell) + \tilde{\mathbf{C}}_{k,\text{VV}}^z(\ell) + \tilde{\mathbf{R}}_{k,\text{V}})^{-1} \tilde{\mathbf{s}}_{k,\text{V}}}{\sum_{i=0}^{K-1} \tilde{\mathbf{s}}_{i,\text{V}}^H (\tilde{\mathbf{C}}_{i,\text{VH}}(\ell) + \tilde{\mathbf{C}}_{i,\text{VV}}^z(\ell) + \tilde{\mathbf{R}}_{i,\text{V}})^{-1} \tilde{\mathbf{s}}_{i,\text{V}}} \quad (23)$$

where $\tilde{\mathbf{R}}_{k,H} = E[\tilde{\mathbf{u}}_{k,H}(\ell)\tilde{\mathbf{u}}_{k,H}^H(\ell)]$ and $\tilde{\mathbf{R}}_{k,V} = E[\tilde{\mathbf{u}}_{k,V}(\ell)\tilde{\mathbf{u}}_{k,V}^H(\ell)]$ are the k th, $M/K \times M/K$ decimated temporal noise covariance matrices for the horizontal and vertical receive polarizations, respectively. The k th decimated structured correlation matrices for the co-pole and cross-pole components are

$$\tilde{\mathbf{C}}_{k,HH}(\ell) = \sum_{\tau=-M+1}^{M-1} \rho_{HH}(\ell + \tau) \tilde{\mathbf{s}}_{k,H,\tau} \tilde{\mathbf{s}}_{k,H,\tau}^H \quad (24)$$

$$\tilde{\mathbf{C}}_{k,HV}(\ell) = \sum_{\tau=-M+1}^{M-1} \rho_{HV}(\ell + \tau) \tilde{\mathbf{s}}_{k,V,\tau} \tilde{\mathbf{s}}_{k,V,\tau}^H \quad (25)$$

$$\tilde{\mathbf{C}}_{k,VH}(\ell) = \sum_{\tau=-M+1}^{M-1} \rho_{VH}(\ell + \tau) \tilde{\mathbf{s}}_{k,H,\tau} \tilde{\mathbf{s}}_{k,H,\tau}^H \quad (26)$$

$$\tilde{\mathbf{C}}_{k,VV}(\ell) = \sum_{\tau=-M+1}^{M-1} \rho_{VV}(\ell + \tau) \tilde{\mathbf{s}}_{k,V,\tau} \tilde{\mathbf{s}}_{k,V,\tau}^H \quad (27)$$

in which the terms $\rho_{HH}(\ell) = E[|x_{HH}(\ell)|^2]$, $\rho_{HV}(\ell) = E[|x_{HV}(\ell)|^2]$, $\rho_{VH}(\ell) = E[|x_{VH}(\ell)|^2]$, and $\rho_{VV}(\ell) = E[|x_{VV}(\ell)|^2]$ are the expected powers of the scattering responses that PAPC estimates. The vectors $\tilde{\mathbf{s}}_{k,H,\tau}$ and $\tilde{\mathbf{s}}_{k,V,\tau}$ contain τ delay-shifted (and zero-filled) versions of the normalized and down-sampled elements of \mathbf{s}_H and \mathbf{s}_V as

$$\tilde{\mathbf{s}}_{k,H,\tau} = \begin{cases} \begin{bmatrix} s_{H,k-\tau} & s_{H,k-\tau+K} & \cdots & s_{H,k-\tau+K(N-1-\tilde{\tau})} & \mathbf{0}_{1 \times \tilde{\tau}} \end{bmatrix}^T & \text{for } \tau \leq 0 \\ \begin{bmatrix} \mathbf{0}_{1 \times \tilde{\tau}} & s_{H,k-\tau+K\tilde{\tau}} & s_{H,k-\tau+K(\tilde{\tau}+1)} & \cdots & s_{H,k-\tau+K(N-1)} \end{bmatrix}^T & \text{for } \tau > 0 \end{cases} \quad (28)$$

and

$$\tilde{\mathbf{s}}_{k,V,\tau} = \begin{cases} \begin{bmatrix} s_{V,k-\tau} & s_{V,k-\tau+K} & \cdots & s_{V,k-\tau+K(N-1-\tilde{\tau})} & \mathbf{0}_{1 \times \tilde{\tau}} \end{bmatrix}^T & \text{for } \tau \leq 0 \\ \begin{bmatrix} \mathbf{0}_{1 \times \tilde{\tau}} & s_{V,k-\tau+K\tilde{\tau}} & s_{V,k-\tau+K(\tilde{\tau}+1)} & \cdots & s_{V,k-\tau+K(N-1)} \end{bmatrix}^T & \text{for } \tau > 0 \end{cases} \quad (29)$$

for the down-sampled delay factor

$$\tilde{\tau} = \begin{cases} \left\lfloor \frac{k-\tau}{K} \right\rfloor & \text{for } \tau \leq 0 \\ \left\lfloor \frac{K-1-(k-\tau)}{K} \right\rfloor & \text{for } \tau > 0 \end{cases} \quad (30)$$

and $\lfloor \bullet \rfloor$ denoting the floor operation.

The superscript $(\bullet)^\circ$ in (20) – (23) denotes an additional modification to the formulation of the structured covariance matrices whereby the $K-1$ range indices on either side of the current range index ℓ in (24) – (27) are set to zero. This “beamspoilage” procedure prevents PAPC from forcing a super-resolution condition [15] that would otherwise degrade sensitivity. It should be noted that this procedure creates a trade-off between resolution and sidelobe suppression that is dependent on the number of range indices that are zeroed on either side of the ℓ th range index.

IV. EXPERIMENTAL RESULTS

The efficacy of PAPC was tested in an open-air experiment using two co-located, dual-polarized Vivaldi antennas for simultaneous transmit and receive (Fig 4). A trihedral and a dihedral at a tilt of 45° were each separately placed at the location of the corner reflector shown in the field of view in Fig. 5. The corner reflector was placed at a range of ~ 97 meters. There is also a variety of others scatterers that include a small sculpture at a range of ~ 3.5 meters, a large steel sculpture having a height of 11.7 meters and width of 7.3 meters at a range of ~ 118 meters that appears as an extended scatterer (Fig. 6) and Nichols Hall itself. The map is sectioned by the 3-dB beamwidth of the horizontally polarized antenna ($\sim 30^\circ$).



Figure 4. Experimental Setup

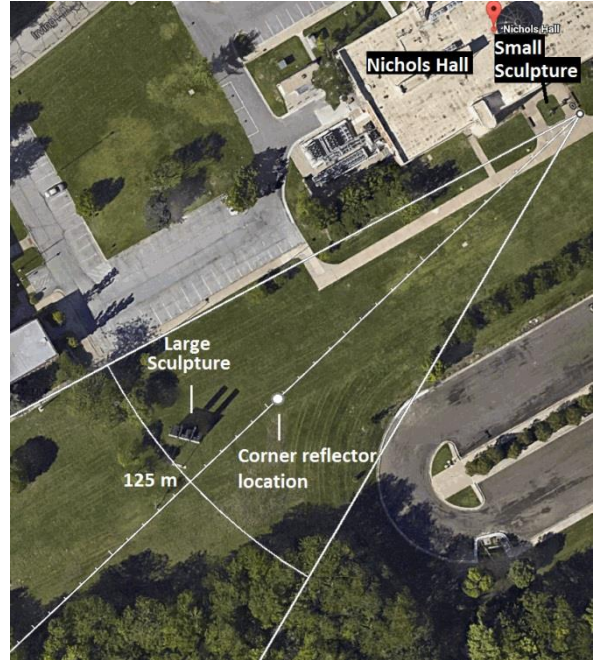


Figure 5. Field of view for polarimetric data collection (Google Maps)



Figure 6. Corner reflector with “Salina Piece” steel sculpture behind

The transmission structure chosen for this test is without the hybrid coupler such that the waveforms are directly connected to the horizontal and vertical channels. This emission structure constrains the resulting emission to the great circle on the Poincaré sphere shown in Fig. 3c. An up-chirp and a down-chirp were chosen as the waveforms for the horizontal and vertical transmit channels, respectively, to provide a comparison of PAPC against matched filtering using a well-known dual-pol transmission scheme.

The LFM waveforms have a time-bandwidth product $BT = 100$ and pulsewidth of 500 ns. The center frequency used is 3.4 GHz with a 3-dB bandwidth of 200 MHz resulting in a range resolution of 0.75 m. The cross-port isolation of the antennas at this frequency is 39 dB. Using matched 27 dB power amplifiers on each channel with approximately 24 dBm per channel results in a total radiated power of 27 dBm. The dual-polarized receive signal is captured directly as $y_H(t)$ and $y_V(t)$. The initial matched filter estimate was obtained using discretized versions of $s_H(t)$ and $s_V(t)$. The data were resampled to $K = 5$ times the bandwidth of the signal using a 1000 point FIR filter. Four range indices were zeroed on either side of the current range index when constructing the PAPC covariance matrices denoted with the superscript $(\bullet)^z$, thus yielding the nominal (matched filter) resolution in range. Four iterations of PAPC were employed.

An additional test case was also implemented by transmitting an optimized waveform in both horizontal and vertical polarizations separated in time, with the first dwell period transmitted horizontal and the next dwell period transmitted vertical. Separating the polarized emissions in time has the effect of decoupling the scattering parameters allowing for reliable estimation. This test serves as a benchmark to compare the matched filter and PAPC estimates in terms of their ability to resolve scatterers. It should be noted that this test was taken at a different times than the dual-polarized emission therefore the range profile is not

guaranteed to be stationary over the entire time period, however large scatterers are present during all tests.

For the time-separated benchmark test the “ultra-low sidelobe” (ULS) waveform from [10] was employed which has an approximate time-bandwidth of 100 with a pulsewidth of 500 ns and approximate bandwidth of 200 MHz. The ULS waveform is demonstrated in [10] to achieve range sidelobes below -80 dB with only a quarter dB of SNR loss and range resolution roughly 30% greater than the LFM waveform.

For comparison, the ideal normalized scattering matrices for the two corner reflector arrangements are

$$\tilde{X}_{\text{dihedral}, 45^\circ} = \begin{bmatrix} 0 & 1 \\ 1 & 0 \end{bmatrix} \quad (28)$$

$$\tilde{X}_{\text{trihedral}} = \begin{bmatrix} 1 & 0 \\ 0 & 1 \end{bmatrix}. \quad (29)$$

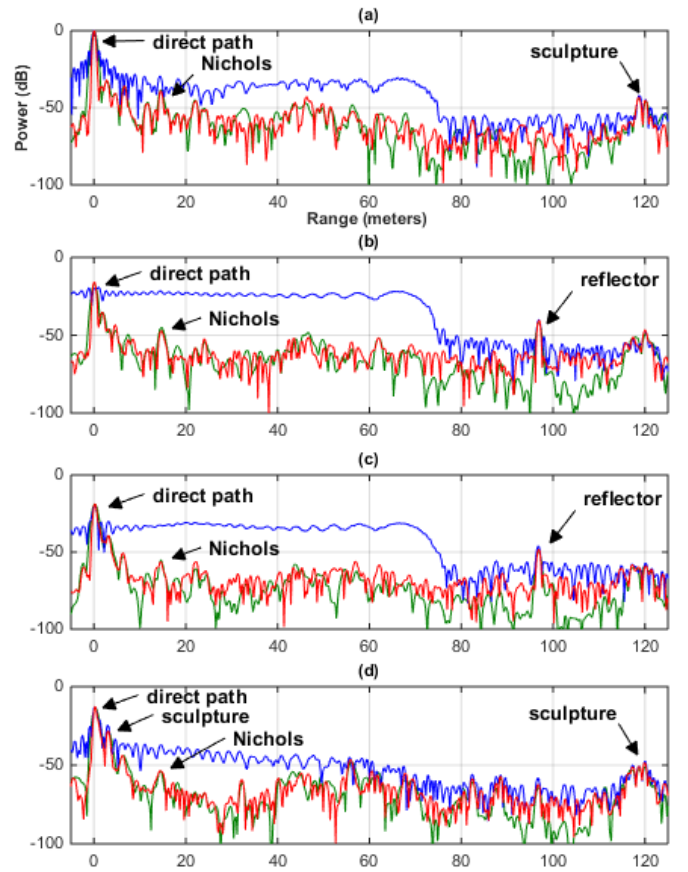


Figure 7. Scattering estimates for the dihedral: (a) $|x_{HH}(\ell)|^2$; (b) $|x_{HV}(\ell)|^2$; (c) $|x_{VH}(\ell)|^2$; (d) $|x_{VV}(\ell)|^2$. Matched Filter (blue), PAPC (red) and ULS (black).

Figures 7 and 8 show the matched filter, PAPC, and ULS processed data for the two reflector arrangements. In Fig. 7 the dihedral reflector is clearly observed in the HV and VH panels and the large sculpture is visible in the HH and VV

panels. Comparing the PAPC results against the matched filter and ULS estimates reveals the ability of PAPC to suppress sidelobes and clearly resolve targets. This suppression is most noticeable in the sidelobes that appear due to the direct path where the PAPC estimate converges from the matched filter initialization to being comparable to the decoupled ULS estimate, suppressing up to 40 dB at some points. The direct path sidelobe suppression reveals the small sculpture in the VV panel at ~ 3.5 meters and what is assumed to be a facet of Nichols Hall at a range of 15 m across all scattering parameters. Note that while the suppression of autocorrelation and cross-correlation sidelobes is quite large at some points, the suppression does not converge to levels comparable to the ULS estimate at greater distances. The cause of this effect is being investigated.

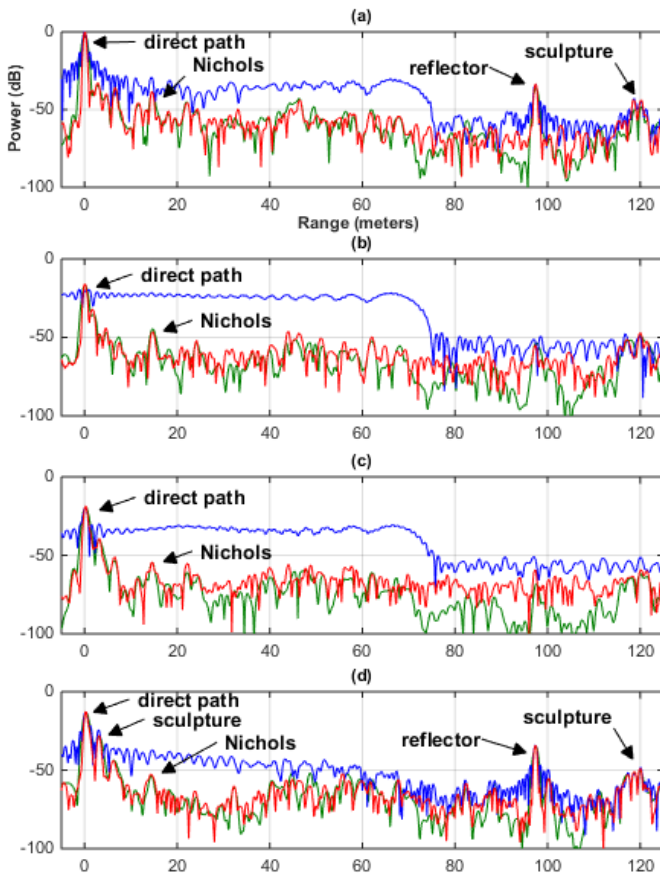


Figure 8. Scattering estimates for trihedral: (a) $|x_{HH}(\ell)|^2$; (b) $|x_{HV}(\ell)|^2$; (c) $|x_{VH}(\ell)|^2$; (d) $|x_{VV}(\ell)|^2$. Matched Filter (blue), PAPC (red) and ULS (black).

Figure 8 illustrates the case where the corner reflector is a trihedral. The HH and VV components of the corner reflector are now observed and PAPC once again demonstrates performance gains over the matched filter. Similar to the previous example, the sidelobes that appear due to the direct path in the matched filter estimate are suppressed to the level of the decoupled ULS estimate using PAPC. This suppression again reveals the small sculpture and Nichols Hall reflection.

CONCLUSIONS

A scheme for controlling polarization modulation in fast-time has been demonstrated that provides the freedom to develop new dual-pol emissions for myriad sensing applications. To address the limitation of waveform cross-correlation on sensitivity, a polarimetric form of adaptive pulse compression has also been derived and experimentally demonstrated to suppress co-pol and cross-pol range sidelobes. A combination of the proposed transmission scheme and PAPC allows for improved estimation of scattering parameters using a selection of polarization diverse emissions.

REFERENCES

- [1] S.D. Blunt, M. Cook, J. Jakabosky, J. de Graaf, and E. Perrins, "Polyphase-coded FM (PCFM) radar waveforms, part I: implementation," *IEEE Trans. AES*, vol. 50, no. 3, pp. 2218-2229, July 2014.
- [2] J.B. Anderson, T. Aulin, and C.-E. Sundberg, *Digital Phase Modulation*, Plenum Press, New York, NY, 1986.
- [3] S.D. Blunt, J. Jakabosky, M. Cook, J. Stiles, S. Seguin, and E.L. Mokole, "Polyphase-coded FM (PCFM) radar waveforms, part II: optimization," *IEEE Trans. AES*, vol. 50, no. 3, pp. 2230-2241, July 2014.
- [4] D. Giuli, "Polarization diversity in radars," *IEE Proceedings*, vol. 74, no. 2, pp. 245-269, Feb. 1986
- [5] V.N. Bringi and V. Chandrasekar, *Polarimetric Doppler Weather Radar: Principles and Applications*, Cambridge, U.K.: Cambridge Univ. Press, 2001.
- [6] J.J. van Zyl and Y. Kim, *Synthetic Aperture Radar Polarimetry*, John Wiley & Sons, Inc., November 2011.
- [7] D. Giuli, L. Facheris, M. Fossi, and A. Rossetini, "Simultaneous scattering matrix measurement through signal coding," *IEEE Intl. Radar Conf.*, Arlington, VA, pp. 258-262, May 1990.
- [8] D. Giuli, M. Fossi, and L. Facheris, "Radar target scattering matrix measurement through orthogonal signals," *IEE Proceedings F: Radar and Signal Processing*, vol. 140, no. 4, pp. 233-242, Aug. 1993.
- [9] S.D. Blunt and K.R. Gerlach, "Multistatic adaptive pulse compression", *IEEE Trans. AES*, vol. 42, no. 3, pp. 891-903, July 2006
- [10] J. Jakabosky, S.D. Blunt, and T. Higgins, "Ultra-low sidelobe waveform design via spectral shaping and LINC transmit architecture," *IEEE Intl. Radar Conf.*, Arlington, VA, 11-15 May 2015.
- [11] L. Ryan, J. Jakabosky, S.D. Blunt, C. Allen, and L. Cohen, "Optimizing polyphase-coded FM waveforms within a LINC transmit architecture," *IEEE Radar Conf.*, Cincinnati, OH, May 2014.
- [12] D. Henke, P. McCormick, S.D. Blunt, and T. Higgins, "The impact of range straddling on least-squares mismatched filtering and adaptive pulse compression," *IEEE Intl. Radar Conf.*, Arlington, VA, 11-15 May 2015.
- [13] S. D. Blunt and T. Higgins, "Dimensionality reduction techniques for efficient adaptive pulse compression," *IEEE Transactions AES*, vol. 46, no. 1, pp. 349-362, 2010.
- [14] T. Higgins, S.D. Blunt, and K. Gerlach, "Gain-constrained adaptive pulse compression via an MVDR framework," *IEEE Radar Conf.*, Pasadena, CA, May 2009.
- [15] S.D. Blunt, K. Gerlach, and T. Higgins, "Aspects of radar range super-resolution," *IEEE Radar Conf.*, Waltham, MA, pp. 683-687, Apr. 2007.